Droop-Inspired Nonlinear Control of a DC Microgrid for Integration of Electrical Mobility Providing Ancillary Services to the AC Main Grid

Miguel Jiménez Carrizosa, Alessio Iovine, *Member, IEEE*, Gilney Damm, *Member, IEEE*, and Pedro Alou, *Member, IEEE*

***Abstract*—The present paper describes an Electric Vehicle (EV) charging station that provides ancillary services to the main AC grid, as for example frequency support and synthetic inertia. Due to the Direct Current (DC) nature of these loads and the easier integration of renewable energies, a DC Microgrid is considered to power the charging station. Targeting both DC grid voltage stability and the capability to support the main AC grid, nonlinear control laws based on Lyapunov theory and backstepping are developed for local and primary control levels (droop control). The proposed controllers are validated via MATLAB-Simulink simulations in a 25 kW DC Microgrid with PV production, Vehicle to Grid (V2G) mode of operation, fast and slow vehicle charge, ancillary services to the AC main grid and islanded mode operation.**

***Index Terms*—DC Microgrid, Vehicle to Grid (V2G), Lyapunov methods, grid stability, large signal analysis.**

I. Introduction

THE FUTURE massive integration of Electric Vehicles (EVs) in the electrical grid represents a significant challenge. The necessity of increasing the power capacity or the adaptation of classical generation units will require considerable financial outlays. Moreover, EVs will demand the creation of a large number of new infrastructures at distribution level, specially charging stations. At the same time, integration of renewable energies in the electrical grid is increasingly prominent, and although they are key actors to reach the climate objectives, their presence in electrical networks represent a major technological challenge from the control point of view. The intermittent nature of renewable energies brings several stability issues and congestion, sometimes even accumulating with similar effects from electric vehicles [1].

Direct Current (DC) Microgrids can help to support the existing electrical network at distribution level thanks to the Vehicle to Grid (V2G) concept. Rather than Alternate Current (AC) grids, they present several advantages such as absence of reactive power and skin effect in the cables, and favour an easier integration of renewable energies and modern loads as battery EVs due to their DC nature [2]. Indeed, they allow to shift towards a more sustainable and reliable electric power system, thanks to their capability to be disconnected and to work in islanded mode, that increases resilience [3]. Moreover, thanks to V2G mode of operation, the batteries of EVs can support electrical grids to regulate their frequency, voltage or reactive power by providing energy to the grid when the vehicles are parked [4], [5]. Since a vehicle is estimated to circulate only between 5% and 10% of daily time [6], [7], it is possible to consider the connected vehicles as power storage elements for the main grid. Consequently, the DC Microgrids can contribute to face the problems related to the inertia reduction due to renewable energy utilisation and EVs integration, by means of proper control techniques as Virtual Inertia [8], [9].

The present paper addresses the problem to ease the integration of EVs via reducing their impact on the grid. Indeed, the increase in number of EVs and the opportunity to consider their batteries for grid stabilization purposes opens up the possibility to consider EVs and charging stations connected via a DC Microgrid for both ensuring stability of the DC Microgrid itself and providing ancillary services to the AC main grid (frequency, inertia, reactive power or voltage support). Nowadays, DC Microgrids are capable to provide these services only when including sufficiently big storage devices [10]. Besides, the proposed grid topology and control approach, enable the DC Microgrid to compensate the lack of big storage devices and to provide support to the AC grid. This will avoid the need for building large infrastructures and consequent high maintenance costs, while allowing the current AC grid to cope with the massive arrival of EVs and renewable energies.

Manuscript received 15 April 2021; revised 10 September 2021 and 20 December 2021; accepted 22 February 2022. Date of publication 4 March 2022; date of current version 23 August 2022. This work was supported by the Spanish Government (Ministerio de Ciencia e Innovacion) through the research project Wi-Batt, "Integration of battery Electric Vehicles into the Energy System: Distributed Control of the DC Microgrid and Bidirectional Wireless Charging Capability," under Grant PID2020-117582RB-I00. Paper no. TSG-00579-2021. *(Corresponding author: Miguel Jiménez Carrizosa.)*

Miguel Jiménez Carrizosa and Pedro Alou are with the Centro de Electrónica Industrial, Universidad Politécnica de Madrid, 28006 Madrid, Spain (e-mail: miguel.jimenezcarrizosa@upm.es; pedro.alou@upm.es).

Alessio Iovine is with the CNRS and Laboratoire des Signaux et Systèmes, CentraleSupélec, Université Paris-Saclay, 91190 Gif-sur-Yvette, France (e-mail: alessio.iovine@l2s.centralesupelec.fr).

Gilney Damm is with COSYS-LISIS, Univ. Gustave Eiffel, IFSTTAR, 77447 Marne-la-Vallée, France (e-mail: gilney.damm@univ-eiffel.fr).

Color versions of one or more figures in this article are available at https://doi.org/10.1109/TSG.2022.3156693.

Digital Object Identifier 10.1109/TSG.2022.3156693

To exchange power in a reliable way, DC Microgrid voltage stability must be guaranteed under adverse circumstances [11]. To guarantee robustness, safety, reliability, and energy efficiency, a hierarchical control strategy is usually implemented [12]. Typically, this includes local, primary, secondary and tertiary controllers, each one with different time scales [13]. Tertiary control, which is related with energy market, and secondary control, which deals with the energy optimal management, are out of the scope of this work. Several results on managing the energy of EVs connected to distribution and transmission systems are available in the literature, as [14], [15], [16], [17]. On the contrary, given the optimal setpoints for the primary and local controllers by the secondary and tertiary ones, fewer results are available on the stability analysis at lower control levels of EVs, especially when no other storage devices are considered [10]. The control strategy proposed in the present paper is composed by primary and local controllers, and targets to ensure short-term stability [13] while the EVs provide ancillary services. Nonlinear local controllers are suggested, and the classical primary control technique named droop control is adapted to them, thus resulting in droop-inspired nonlinear controllers.

Local controllers for each power converter are dedicated to control current or voltage in the order of milliseconds, and are usually implemented as Proportional Integral (PI) controllers, e.g., [18]. When they are developed via linearization techniques, the dedicated stability analysis is a small signal one, while large signal stability can be ensured if nonlinear control techniques are considered.

Droop control is typically used for primary control to assure a steady-state load sharing, where the power converters adjust their output voltages when output currents change. Different types of droop characteristic (including inversed droop, non-linear droop, and adaptive droop) have been investigated recently apart from the conventional linear droop control [19]. For example, in [20] a generic polynomial expression is presented to unify different nonlinear droop control as parabola, inverse parabola, ellipse or 5^{th} order polynomial. However, some of them present stability problems in case of heavy constant power loads (CPL). In [21], the authors introduce a dead-band droop for the correct management of the energy in the batteries that varies their charging capability with respect to their State of Charge (SoC). In [22], a fuzzy control with gain-scheduling technique is addressed for DC voltage regulation of multi-phase DC/DC converters. Nonetheless, the tuning of this type of controllers in real implementation is not trivial, and "trial and error" methods need to be used. In [23], the authors suggest an adaptive and decentralized power sharing approach taking into account the line impedance; since it considers PI controllers, it easily generates problems when the system does not work near the equilibrium point. Primary control stability for droop control techniques is still an open problem in the current literature [24].

The present paper leverages and adapts results on control techniques [9], [18], [24] to the case of charging stations for EVs with no storage devices dedicated to ensure stability and power quality [10], thus reducing the impact of EVs on the grid and paving their way to participate in the market of ancillary services. Indeed, the proposed local and primary controllers for a DC Microgrid connecting charging stations for EVs ensure large signal stability with respect to power variations while extracting renewable power from PV arrays and providing frequency support to a connected AC grid, without the necessity for extra storage devices. According to the nature of the power source, nonlinear and scalable local control laws for buck or boost are suggested based on backstepping [25], as well as for Dual Active Bridge (DAB) converters. In order to allow for the possibility to operate in islanded more or connected to the main grid, three types of control modes are foreseen for the bidirectional battery chargers of EVs: i) current charge, ii) voltage charge and iii) DC grid voltage control. A stability analysis based on Lyapunov theory [25], [26], [27] is provided by tuning the primary droop controllers' gains, to the purpose to ensure proper DC bus regulation and power quality. The proposed results are scalable to any (finite) number of components for the selected Microgrid. Finally, the periodical adaptation of the droop gains depending on the mode of operation at each node ensure the possibility to use the EVs for stability purposes, both for the DC Microgrids connecting the charging stations and the AC main grid. Thanks to the proposed solution, both sustainable mobility and integration of renewable energies in the electrical grid can be combined while guaranteeing the stability of the system at all times with no need to oversize the storage elements.

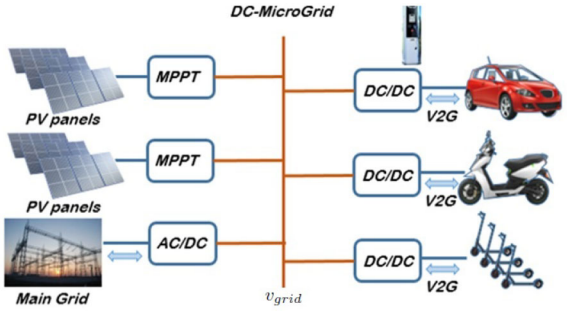

Fig. 1. The considered DC Microgrid for EVs integration.

The proposed analysis is tested in MATLAB/Simulink environment: both theoretical analysis and simulation results show the effectiveness of the proposed solution, such to favour the utilisation of DC Microgrids as charging stations for EVs.

The rest of the paper is organized as follows: in Section II we introduce the modeling of the subsystems composing the Microgrid. Section III introduces the control approach, and results are provided in Section IV. Section V outlines the conclusive remarks.

II. DC Microgrid Model

The considered DC Microgrid dedicated to EV recharge is depicted in Figure 1: it is composed by renewable energy sources as photovoltaic panels, storage systems represented by the EVs, and the connection with the main AC grid. For each component of the Microgrid and the connection to the AC grid, a converter ensures the connection; bidirectional Dual Active Bridge (DAB) converters are considered for EV; unidirectional

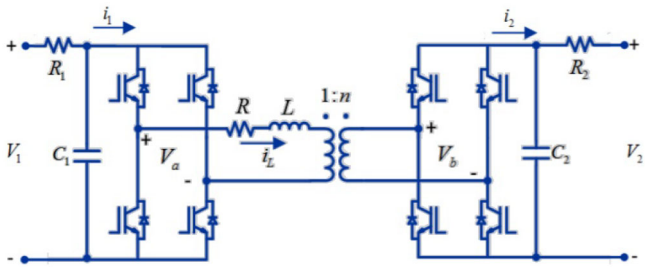

Fig. 2. Electrical scheme of the bidirectional DAB converter.

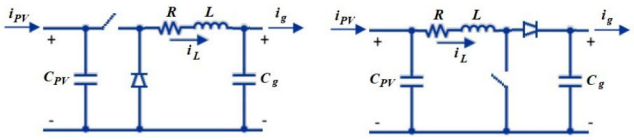

Fig. 3. a) Buck converter b) Boost converter.

DC/DC buck or boost converters for PV arrays; an AC/DC bidirectional converter is used for proper connection with the AC grid. The models are obtained using averaging technique with Pulsed Width Modulation (PWM) [28]. In the sequel, the models for each subsystem composing the Microgrid are described.

A. Converter for EVs

In order to properly control the energy charge and discharge for EVs, bidirectional Dual Active Bridge (DAB) converters are used. They are chosen due to their important advantages as soft-switching commutations, galvanic isolation, low cost, high efficiency and the need for a reduced number of devices [29]. The DAB electrical scheme is shown in Figure 2 and its nonlinear model (see [30]) is shown in equations (1a)-(1c):

$$\dot{i}_1 = -\frac{R}{L}\cdot i_1 + \frac{T\cdot R\cdot n}{L^2}\cdot d\cdot(1-2|d|)\cdot v_{C_2} \tag{1a}$$

$$\dot{v}_{C_1} = -\frac{1}{C_1}\cdot i_1 - \frac{1}{R_1 C_1}\cdot v_{C_1} + \frac{V_1}{R_1 C_1} \tag{1b}$$

$$\dot{v}_{C_2} = \frac{n}{C_2}\cdot i_1 - \frac{1}{R_2 C_2}\cdot v_{C_2} + \frac{V_2}{R_2 C_2} \tag{1c}$$

where v_{c_1} and v_{c_2} are the voltages of the input and output capacitors C_1 and C_2, respectively; i_1 is the input current in the converter; V_1 is the battery voltage; V_2 the grid voltage; T is the switching period; n is the transformer ratio; and d is the duty cycle (control variable). R is the resistance in the inductance L, while R_1 and R_2 are the ones connecting the battery and the grid to the converter, respectively.

B. Converter for PV Panels

The PV arrays are the main power sources in the considered DC Microgrid, and are desired to work according to Maximum Power Point Tracking (MPPT) algorithms. Unidirectional buck or boost DC/DC converters are used, depending on the voltage level of the DC Microgrid and the PV panels. Figure 3 describes the considered electrical schemes: $v_{C_{PV}}$ and v_g are the voltages of the input and output capacitors C_{PV} and C_g, respectively; i_L is the current on the inductance L; and R is its resistance.

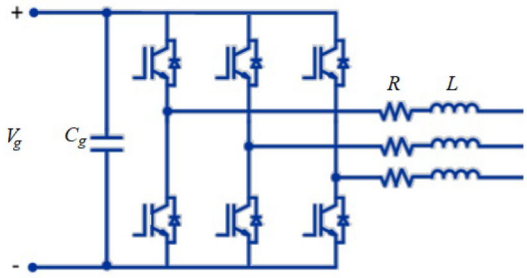

Fig. 4. AC/DC bidirectional converter.

The resulting model for a Buck and for a Boost converters are described in equations (2) and (3), respectively:

$$\dot{i}_L = -\frac{R}{L}\cdot i_L + \frac{d}{L}\cdot v_{C_{PV}} - \frac{1}{L}\cdot v_{C_g} \tag{2a}$$

$$\dot{v}_{C_{PV}} = \frac{I_{PV}}{C_{PV}}\cdot -\frac{d}{C_{PV}}\cdot i_L \tag{2b}$$

$$\dot{v}_g = \frac{1}{C_g}\cdot i_L - \frac{1}{C_g}\cdot i_g \tag{2c}$$

$$\dot{i}_L = -\frac{R}{L}\cdot i_L + \frac{1}{L}\cdot v_{C_{PV}} - \frac{d}{L}\cdot v_{C_g} \tag{3a}$$

$$\dot{v}_{C_{PV}} = \frac{I_{PV}}{C_{PV}}\cdot -\frac{d}{C_{PV}}\cdot i_L \tag{3b}$$

$$\dot{v}_g = \frac{d}{C_g}\cdot i_L - \frac{1}{C_g}\cdot i_g \tag{3c}$$

where d is the duty cycle, i_g is the current through the DC Microgrid and I_{PV} is the current provided by the solar panel, which is defined as:

$$I_{PV} = I_{pv} - I_0\cdot\left(e^{\frac{qV}{KT}-1}\right) - \frac{V+IR_s}{R_s} \tag{4}$$

where I_{pv} is the irradiance generated current, I_0 is the diode saturation current, q is the electron charge, K is the Boltzman constant, T is the cell temperature in Kelvin, V is the solar cell output voltage and R_s is the solar cell series resistance.

C. Converter for Connection With AC Grid

The connection with a main AC grid is ensured via a three phases AC/DC bidirectional Voltage Source Converter (see Figure 4).

The $dq0$ frame has been used to model the system. As one of the goals is to provide frequency support to the AC grid, the frequency ω has also been modeled, together with the AC currents i_d, i_q, i_0, and the voltages v_d, v_q, v_0 in the $dq0$ frame. C_g is the capacitor, while L and R are the inductance and resistance, respectively. The dynamical model is:

$$\dot{i}_d = -\frac{R}{L}\cdot i_d - \omega\cdot i_q - M_d\cdot v_g + v_d \tag{5a}$$

$$\dot{i}_q = \omega\cdot i_d - \frac{R}{L}\cdot i_d - M_q\cdot v_g + v_q \tag{5b}$$

$$\dot{i}_0 = -\frac{R}{L}\cdot i_0 + v_0 \tag{5c}$$

$$\dot{v}_g = -\frac{3}{2C_g \cdot v_g}\left(v_d i_d + v_q i_q + v_0 i_0\right) + \frac{1}{C_g} \cdot i_l \tag{5d}$$

$$\dot{\omega} = \Lambda\left[P_m - \frac{3}{2}\left(v_d i_d + v_q i_q + v_0 i_0\right)\right] \tag{5e}$$

where P_m is the total input mechanic power supplied by the AC sources. The term Λ depends on the inertia of all the AC synchronous generators, and v_g is the voltage at DC side in the converter.

D. DC Common Bus

We consider the DC Microgrid in Figure 1 to have a common DC bus, which voltage is represented by v_{grid}, that connects the set of devices in Sections II-A, II-B and II-C. Such voltage is impacted by the flowing power/current from/to the several subsystems composing the Microgrid, and by how the power unbalance is managed. While PV arrays and the interconnections with the AC grid are always controlled in terms of references for power input/output, we need to differentiate three control modes for the EVs. Indeed, according to control target, we need to consider:

i battery current control mode (for both slow as fast charging); a current reference is selected such to impose a desired recharge profile.

ii battery voltage control mode; it targets to properly control the last steps of its charger (usually used when State-of-Charge (SoC) is more than 80%) [31]. The voltage reference provided by manufacturer is selected for ensuring a safe desired charging profile.

iii DC grid voltage control mode; the energy is used according to the needs of the DC grid, acting as primary control actuators and ensuring power quality by droop control. A reference $v^*_{DC,i}$ will be provided by secondary controller.

Then, it is straightforward to model the power variations on the DC bus accordingly. The dynamic of v_{grid} is:

$$\dot{v}_{grid} = \frac{1}{C_{grid}}\left(\Psi + \sum_{j \in droop} \frac{v_{g,j} - v_{grid}}{R_{g,j}}\right) \tag{6}$$

where:

$$\Psi = \sum_{p \in PV} i_{pv} - \sum_{a \in AC} i_{ac} + \sum_{b \in bat} \frac{v_{g,b} - v_{grid}}{R_{g_b}} \tag{7}$$

The second term on the right-side in (6) describes the current provided by the devices that are dedicated to ensure DC bus voltage stability via droop control. In (6), p is the number of the PV arrays, a the number of connections with the AC main grid, j the number of batteries in droop control mode (mode iii) and b the number of batteries in both charging modes (current -mode i- or voltage -mode ii-). It is important to remark that the voltages $v_{g,j}$ and $v_{g,b}$ are the DC Microgrid side voltages of the DAB converters associated to the EVs in droop mode or charging mode, respectively. Finally, C_{grid} is the capacitor at DC common bus, that represents the capacitances from cables of DC Microgrid.

III. DC Microgrid Control

This section describes nonlinear control law design based on Lyapunov stability theory for each subsystem composing the microgrid. We first consider the control laws for PV arrays, interconnection with the AC grid, and EVs in battery recharge mode, both current or voltage (mode i and ii). We name them as local control laws. Then, we provide control laws for the EVs in charge of DC bus voltage regulation, then operating as primary control. The aforementioned control laws are developed according to Lyapunov stability analysis. Indeed, to the purpose to obtain a stability result for the interconnected system, a mathematical analysis based on a composition of Lyapunov functions is provided. In the present work, some insights raised in [18] for a different topology of DC Microgrids are pursued and developed for the EV charging station case. Furthermore, the possibility to switch the control mode for the EVs is envisaged.

A. Local Controllers

1) Battery Current Control Mode: referring to the electrical scheme in Figure 2, we consider here the given current reference i_{1ref} for the variable i_1 in equation (1a). We define a candidate Lyapunov function as:

$$W_{i_1} = \frac{1}{2}\left(i_1 - i_{1ref}\right)^2 \tag{8}$$

and compute its time derivative as:

$$\dot{W}_{i_1} = \left(\left(i_1 - i_{1ref}\right) \cdot \left(\frac{T \cdot R \cdot n}{L^2} \cdot d \cdot (1 - 2|d|\right) \cdot v_{C_2}\right) + \left(i_1 - i_{1ref}\right) \cdot \left(-\frac{R}{L} \cdot i_1 - \dot{i}_{1ref}\right) \tag{9}$$

To effectively track the desired reference, a negative definite time derivative of the form:

$$\dot{W}_{i_1} = -\alpha\left(i_1 - i_{1ref}\right) \tag{10}$$

is envisaged, with $\alpha > 0$. To this purpose, we target to have:

$$-\frac{R}{L} \cdot i_1 + \frac{T \cdot R \cdot n}{L^2} \cdot d \cdot (1 - 2|d|) \cdot v_{C_2} - \dot{i}_{1ref} = -\alpha\left(i_1 - i_{1ref}\right) \tag{11}$$

Then, we select the duty cycle ($-0.5 \leq d \leq 0.5$) as:

$$d = \frac{1 - \sqrt{1 - 8A}}{4} \cdot S_1 + \frac{-1 + \sqrt{1 + 8A}}{4} \cdot S_2 \tag{12}$$

where:

$$A = \frac{nL^2}{RTv_{C_2}}\left[-\alpha\left(i_1 - i_{1ref}\right) + \dot{i}_{1ref} + \frac{R}{L} i_1\right] \tag{13}$$

and $S_1 = 1$, $S_2 = 0$ if $i_{1ref} > 0$, or $S_1 = 0$, $S_2 = 1$ if $i_{1ref} < 0$.

Consequently, the time derivative of $\dot{W}_{i_1}$ in (10) is actually negative definite, and asymptotic stability can be ensured for the current with respect to the reference i_{1ref}. Due to the linearity of equations (1b) and (1c), and considering the voltages V_1 and V_2 constant or slowly time-varying, it is easy to verify that these subsystems are stable with respect to their equilibrium points if i_1 is stable, as their eigenvalues are negatives [25, Th. 4.5].

2) Battery Voltage Control Mode: referring to the electrical scheme in Figure 2, we consider here the given constant voltage reference v_{1ref} for the voltage v_{C_1} in equation (1b). Characteristics on when considering this control mode mainly depends on the battery's data sheet, but it is usually applied when the SoC is higher than 80%. To use backstepping theory for developing the control law, we consider the tracking errors between v_{C_1} and its given reference v_{1ref}, and between i_1 and a reference i_{1ref}, that has still to be computed:

$$\tilde{v}_{C_1} = v_{C_1} - v_{1ref}, \quad \tilde{i}_1 = i_1 - i_{1ref} \tag{14}$$

We define a candidate Lyapunov function as:

$$W_1 = W_{v_{C_1}} + W_{i_1} = \frac{C_1}{2}\left(\tilde{v}_{C_1}\right)^2 + \frac{1}{2}\left(\tilde{i}_1\right)^2 \tag{15}$$

Since v_{1ref} is constant, and considering equation (1b), then:

$$\dot{\tilde{v}}_{C_1} = -\frac{1}{C_1}(\tilde{i}_1 + i_{1ref}) - \frac{1}{R_1 C_1}(\tilde{v}_{C_1} + v_{1ref}) + \frac{V_1}{R_1 C_1} \tag{16}$$

Consequently, the time derivative of $W_{v_{C_1}}$ in (15) is:

$$\dot{W}_{v_{C_1}} = \tilde{v}_{C_1} \cdot \left(-i_{1ref} - \frac{\tilde{v}_{C_1} + v_{1ref}}{R_1} + \frac{V_1}{R_1}\right) - \tilde{v}_{C_1}\tilde{i}_1 \tag{17}$$

We select the reference i_{1ref} as:

$$i_{1ref} = \frac{1}{R_1} \cdot \left(\tilde{v}_{C_1} - v_{1ref} + K_1 \cdot \tilde{v}_{C_1}\right) \tag{18}$$

where K_1 is a positive constant gain. Therefore:

$$\dot{W}_{v_{C_1}} = -\left(\frac{1}{R_1} + K_1\right) \cdot \tilde{v}_{C_1}^2 - \tilde{v}_{C_1}\tilde{i}_1 \tag{19}$$

and

$$\begin{aligned}\dot{W}_1 = &-\left(\frac{1}{R_1} + K_1\right) \cdot v_{C_1}^2 - \tilde{v}_{C_1}\tilde{i}_1 + \tilde{i}_1\left(-\dot{i}_{1ref}\right) \\ &+ \tilde{i}_1\left(\frac{T \cdot R \cdot n}{L^2} \cdot d \cdot (1 - 2|d|)\right)v_{C_2} - \left(\frac{R}{L}(\tilde{i}_1 + i_{1ref})\right)\end{aligned} \tag{20}$$

Consequently, we select the duty cycle similarly and (12), by imposing:

$$\begin{aligned}&\frac{T \cdot R \cdot n}{L^2} \cdot d \cdot (1 - 2|d|)v_{C_2} \\ &-\frac{R}{L}\left(\tilde{i}_1 + i_{1ref}\right) - \tilde{v}_{C_1} - \dot{i}_{1ref} = -\alpha\tilde{i}_1\end{aligned} \tag{21}$$

Therefore, the A value in the control input d in (12) is:

$$A = \frac{nL^2}{RTv_{C_2}}\left[-\alpha\tilde{i}_1 + \dot{i}_{1ref} + \tilde{v}_{C_1} + \frac{R}{L}(\tilde{i}_1 + i_{1ref})\right] \tag{22}$$

Finally, the error dynamics $\tilde{v}_{C_1}$ and $\tilde{i}_1$ are asymptotically stable, as it results:

$$\dot{W}_{v_{C_1}} = -\left(\frac{1}{R_1} + K_1\right)\tilde{v}_{C_1}^2 - \alpha\tilde{i}_1^2 \tag{23}$$

The same stability considerations due to the linear nature of v_{C_2} that are stated for the current control mode can here be applied.

3) PV Controller: The control law for the duty cycle d is provided, and we refer to the results described in [18] for more details on the used Lyapunov analysis via backstepping and dynamic feedback linearization that targets to obtain stability proof for converters with MPPT implementation. The control d is:

$$d = \frac{1}{v_g}\left[v_{C_{PV}} - Ri_L + \beta - L\dot{z} + K(i_L - z)\right] \tag{24}$$

where $\beta > 0, K > 0$ are constant control parameters, and z is the reference trajectory for backstepping implementation [18].

4) AC Distribution Bidirectional Controller: Similarly to the PV case, only the control laws dedicated to provide frequency support in dq frame are provided:

$$M_d = \frac{1}{v_g}\left[v_d - Ri_d - L\omega i_q + \alpha - L\dot{z_d} + K_d(i_d - z_d)\right] \tag{25}$$

$$M_q = \frac{1}{v_g}\left[v_q - Ri_q + L\omega i_d - L\dot{z_q} + K_q(i_q - z_q)\right] \tag{26}$$

where α, K_d, K_q, z_d and z_q are defined in [18].

B. Primary Controller

As already stated, the target to ensure DC bus voltage stability is shared among the EVs that are in grid voltage control mode, such to define a droop control framework. The philosophy of droop control technique is that several network nodes share out the responsibility to maintain the DC voltage of the grid at the same time [32]. They react to power imbalance when a power variation in the grid occurs and adjust the amount of power by a set of local proportional controllers with gains (γ_i) (see equation (31)), called droop gains. Primary control is not necessarily implemented in all network nodes, but it is often implemented in nodes where energy reserves exist.

It is important to emphasize that the number of EVs connected to the network will vary over time, as new vehicles will connect to recharge their batteries or the charged ones will disconnect. Moreover, the number of batteries that are in different operating modes can vary as well, as EVs can switch from battery voltage control mode to primary control for DC bus regulation if needed. Therefore, the primary control has to constantly adapt its gains depending on the number of batteries in this operating mode. We consider the secondary control level (not explained in this paper) to manage the switching of the EVs among the different control modes.

1) DC Grid Voltage Control Mode: Let us consider the DC bus equation (6), the DC Microgrid side voltage equation of the DAB converter (1c) and the desired voltage value for the DC bus $v_{grid,ref}$. Let W_{grid} be a candidate Lyapunov function:

$$W_{grid} = \frac{v_{grid}^2}{2}C_{grid} + \sum_{j \in droop}\frac{v_{g,j}^2}{2}C_{g,j} \tag{27}$$

In order to select the proper control inputs such that the primary controller ensures DC bus stability, we consider the time

derivative $\dot{W}_{grid}$ as:

$$\dot{W}_{grid} = v_{grid}\left(\Psi + \sum_{j\in droop} \frac{v_{g,j} - v_{grid}}{R_{g,j}}\right) + \sum_{j\in droop} v_{g,j}\left(i_{2,j} + \frac{v_{grid} - v_{g,j}}{R_{g,j}}\right) \quad (28)$$

where $i_{2,j}$ is the current of the DC grid-side DAB converter of battery j, and Ψ was introduced in (7). By defining the tracking error for $\tilde{i}_{2,j}$ as:

$$\tilde{i}_{2,j} = i_{2,j} - i_{2,jref} \quad (29)$$

it is possible to rewrite (28) as:

$$\dot{W}_{grid} = -\sum_{j\in droop}\left(\frac{v_{grid} - v_{g,j}}{R_{g,j}}\right)^2 + v_{grid}\cdot\Psi + \sum_{j\in droop} v_{g,j}\left(i_{2,jref} + \tilde{i}_{2,j}\right) \quad (30)$$

Consequently, a possible choice for the reference $i_{2,jref}$ is:

$$i_{2,jref} = \frac{\gamma_j}{v_{g,j}}\left[-v_{grid}\Psi - k_j\left(v_{grid}^2 - v_{grid,ref}^2\right)\right] \quad (31)$$

where $\gamma_j \in [0,1]$, $\sum_j \gamma_j = 1$ and $k_j > 0$ are control variables associated with droop control gains. Consequently, the control input d_j is defined as in (12), and the A_j value is:

$$A_j = \frac{n_j L^2}{RTv_{g,j}}\left[-\alpha\tilde{i}_{2,j} + \dot{i}_{2,jref} + v_{g,j} + \frac{R}{L}(\tilde{i}_{2,j} + i_{2,jref})\right] \quad (32)$$

The choice of the different γ_j can be derived considering the different levels of charge of the storage devices, their sizes, the losses in the system, etc. A dedicated higher (secondary) level controller can be defined.

It must be noted that the gains γ_j can be related to the droop gains adopted when performing droop control for slow storage devices [32]. It is then possible to state that the performed control action acts according to the droop control mode. The proposed contribution develops an analytical result for a general case considering devices possibly having different characteristics, with respect to different convergence rates and proper choice of the gains. Being the contribution clearly related to a well known methodology, it can immediately profit of its state-of-the-art development.

C. Stability Analysis

In [18], stability analysis based on Lyapunov function is provided for the subsystems (2), (3), and (5) with respect to a stable DC bus. Complementary, we consider here the existence of control inputs and Lyapunov functions such that the PV array operates correctly in MPPT mode, and that the VSCs connected to the AC grid are able to provide ancillary services as frequency support. Consequently, the main interest now is to show stability of the DC bus, such that the interconnection of the whole set of subsystems is stable. Then, only the DAB converters are taken into account, and the other subsystems are considered as sources of disturbances acting on the DC bus. Among the DAB converters, we distinguish the ones stabilizing the DC bus by primary control, and the ones acting in battery current or voltage control mode. Moreover, we focus on the possibility for the high level controller to switch operating mode for the EVs.

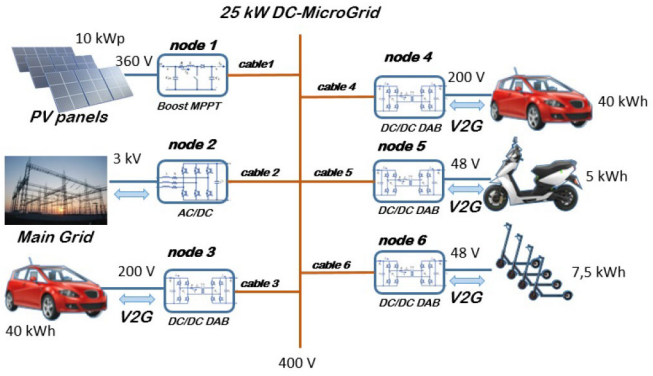

Fig. 5. The 25 kW DC Microgrid.

Let us define the states x_b and x_j as composed by the current and voltage variables of the EVs subsystems in (1), according to their operating mode:

$$x_b = \left[\, i_{1,b} \;\; v_{C_1,b} \;\; v_{g,b} \,\right]^T \forall\, b \in bat \;\; (modes\ i\ \&\ ii) \quad (33)$$

$$x_j = \left[\, i_{1,j} \;\; v_{C_1,j} \;\; v_{g,j} \,\right]^T \forall\, j \in droop \;\; (mode\ iii) \quad (34)$$

Then, let us consider the reference vectors x_b^r and x_j^r as defined by the references i_{1ref} in (8), (18) and (31), and the equilibrium voltages that are obtained by computation of the steady state values of equations (1b) and (1c) in case of $v_{grid} = v_{grid,ref}$. Let the state x and the reference vector x^r be

$$x = \left[x_b \;\; x_j \;\; v_{grid}\right]^T \quad ; \quad x^r = \left[x_b^r \;\; x_j^r \;\; 0\right]^T \quad (35)$$

and consider the error $\tilde{x} = x - x^r$.

Theorem 1: Given $\tilde{x}$ and the current reference for primary control in (31), the control laws d in (12) with respect to A in (13), (22), and (32), ensure grid stability, since there exist suitable functions $\beta_x \in K\mathcal{L}$ and $\beta_v \in K$ such that:

$$\|\tilde{x}(t)\| \le \beta_x(\tilde{x}(0), t) + \beta_v(v_{grid,ref}) \quad (36)$$

Proof: The proof is based on composition of Lyapunov functions. By considering Lyapunov candidate functions as in (9), (15) and (27), and their time derivatives in (10), (23) and (28), it is possible to define a positive definite function W which time derivative $\dot{W}$ is

$$\dot{W} = -\sum_{b\in bat}\left[\alpha\tilde{i}_1^2 + p_1^i\tilde{v}_{C_1}^2 + p_2^i\tilde{v}_{C_2}^2\right] - \sum_{b\in bat}\left[\left(\frac{1}{R_1} + K_1\right)\tilde{v}_{C_1}^2 + \alpha\tilde{i}_1^2 + p_2^{ii}\tilde{v}_{C_2}^2\right] - \sum_{j\in droop}\left[\left(\frac{v_{grid} - v_{g,j}}{R_{g,j}}\right)^2 + \gamma_j k_j v_{grid}^2 - \gamma_j k_j v_{grid,ref}^2\right] \quad (37)$$

where $p_1^i > 0$, $p_2^i > 0$, $p_2^{ii} > 0$ can be computed by Lyapunov equations for the dynamics in (1b) and (1c).

From (37), inequality (36) follows [25], [27]. ■

TABLE I
SIMULATION PARAMETERS

DC Microgrid		**Motorbike chargers**	
Rated power	25 kW	Battery energy	5 kWh
Rated voltage	400 V	Battery voltage	48 V
Cable resistances	0.01 Ω		
PV panels		**Lumped chargers**	
Rated power	10 kWp	Battery energy	7.5 kWh
Rated voltage	360 V	Battery voltage	48 V
Car chargers		**AC grid**	
Battery energy	40 kWh	Rated voltage	3 kV
Battery voltage	200 V	Inertia $[kg \cdot m^2]$	25000

TABLE II
CONVERTERS PARAMETERS

Node 1 (boost converter)	
Inductance	400 mH
Switching frequency	2 kHz
Capacitor (DC Microgrid side)	400 μF
Node 2 (AC/DC)	
Inductances (per phase)	40 mH
Switching frequency	10 kHz
Capacitor (DC Microgrid side)	200 μF
Nodes 3&4 (DAB))	
Inductance	20 mH
Resistance	0.4Ω
Nonlinear control parameter (α)	20
Switching frequency	5 kHz
Capacitor (DC Microgrid side)	400 μF
Transformer ratio (n)	2
Nodes 5&6 (DAB))	
Inductance	1mH
Resistance	0.1Ω
Nonlinear control parameter (α)	10
Switching frequency	500Hz
Capacitor (DC Microgrid side)	400 μF
Transformer ratio (n)	8

For short-term stability purposes [11], Theorem 1 provides stability results for the EVs charging station if at least one EV is connected. However, the capability to ensure long-term stability depends on the SoC and on the ongoing power flow. The same results apply in case of connections and disconnections of EVs, as far as they do not take place in a short time period. Indeed, the resulting system would result to be a hybrid control system, and the existence of a sufficiently large dwell time with respect to the system's dynamics ensure stability [33]. The considered high level controller then allows for plug and play features and a switch for the EVs among their mode, if that switch is slower than a certain threshold.

IV. SIMULATIONS

A 25 kW, 400 V DC Microgrid is considered for simulations in this Section, whose configuration is depicted in Figure 5. The DC Microgrid is composed by a PV solar installation of 10 kWp, a connection to the AC main grid (distribution level at 3 kV), 2 electric car chargers at 200 V, 1 charger for an electric motorbike at 48 V and 1 charger for a lumped load composed of several scooters at 48 V. The parameters of the DC Microgrid are shown in Table I, while Table II shows the converters' ones.

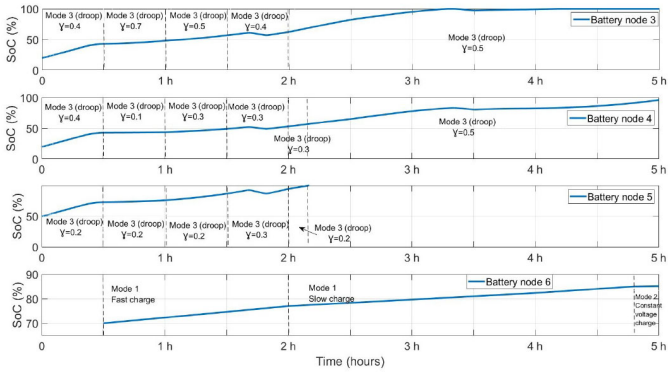

Fig. 6. SoC of the batteries of the EVs at nodes 3, 4, 5 and 6.

A 5 hours simulation is carried out in MATLAB/Simulink environment, considering both the connection to the AC grid and the islanded mode. The goal is to verify robustness of the nonlinear controllers both for local and primary levels in the DC Microgrid. In Figure 6, the SoC of the batteries of the EVs at the nodes 3, 4, 5 and 6 are shown. Initially, we consider the situation where only three EVs are connected to the DC Microgrid: in nodes 3 and 4 the same electric cars are connected with the same initial charge (20%), while in node 5 an electric motorbike is connected with an initial SoC of 50%. The batteries of the aforementioned EVs are in mode 3 (droop control mode), i.e., they are in charge to regulate the voltage of DC Microgrid. (see Figure 8).

A fourth EV battery is connected in node 6 at $t = 30$ minutes; at first, this battery operates in mode 1 (fast current charge), while at $t = 120$ minutes it changes to slow current charge. Finally, at $t = 280$ minutes it reaches the 85% of the SoC and it moves to charge mode 2 with constant voltage. Moreover, at $t = 130$ minutes, the end-user of the motorbike of node 5 disconnect it, thus not allowing it anymore to contribute to the voltage stability of the grid. We remark that the changes in the configuration for the EVs, both in the operating modes and in the droop gains, are computed in secondary and tertiary level controls, which are not considered in this paper, and these controllers will take into account renewable production, weather and load forecast, AC grid ancillary services engagement, etc...

To investigate more cases of interest, the droop gains (γ_i) vary along the simulation time. For example, between $0 \leq t \leq 30$ minutes, we set $\gamma_3 = \gamma_4 = 0.4$. As a consequence, the batteries of these nodes have exactly the same behaviour, as Figures 6 and 7 show. On the contrary, when $30 < t \leq 130$ minutes, we set $\gamma_3 \neq \gamma_4$, and consequently the SoCs have different dynamics. Moreover, we remark that both the connection to the AC grid and the islanded mode are investigated in simulations, as depicted in Figure 10.

Figure 7 shows the power flows in the DC Microgrid. When $0 \leq t \leq 30$ minutes, the solar production is not enough to supply the batteries of the EVs, and therefore the DC Microgrid demands energy to the AC grid. We remark that the batteries at nodes 3 and 4 are maintaining the voltage of the DC grid while absorbing exactly the same power, since they operate with the same constant droop gains. Between $30 < t \leq 100$ minutes,

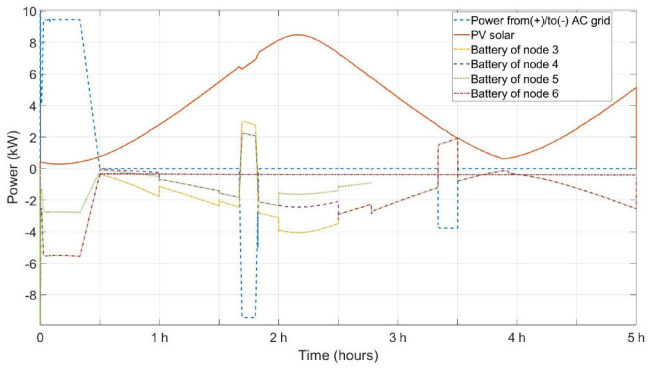

Fig. 7. Powers in DC Microgrid.

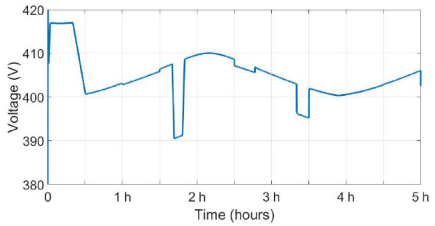

Fig. 8. The voltage of the DC Microgrid.

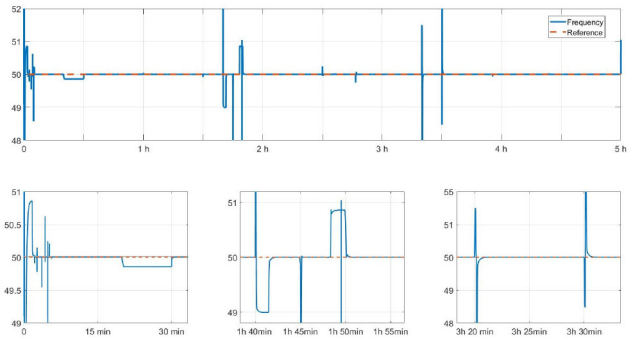

Fig. 9. Frequency in AC grid.

the DC Microgrid operates in islanded mode. Then, no power is demanded or supplied to the AC main grid (the AC/DC converter is disconnected). Next, at $t = 100$ minutes a problem occurs in the AC side and the DC grid starts to supply energy to the AC side to provide frequency support. The batteries in nodes 3, 4 and 5 begin to discharge, and since they have different droop gains their SoCs have different evolutions. Between ($110 \leq t \leq 200$) minutes the DC Microgrid operates again in islanded mode, while at $t = 200$ minutes a new problem arises in the AC grid, and it forces the DC Microgrid to provide frequency support (see Figure 9).

The voltage of the DC Microgrid is shown in Figure 8. Thanks to the proposed droop control, the voltage is always inside the $\pm 4\%$ of rated value (400 V) despite of the variation in the PV solar production, the connection or disconnection of batteries (EVs) in the system and the stability problems that arise in the AC side.

The frequency of the AC grid is shown in Figure 9; it is around 50 Hz, thus correctly tracking its reference despite the introduced problems. We stress that the proposed control strategy allows for a fast restoration of the frequency value, thanks to the support of DC Microgrid.

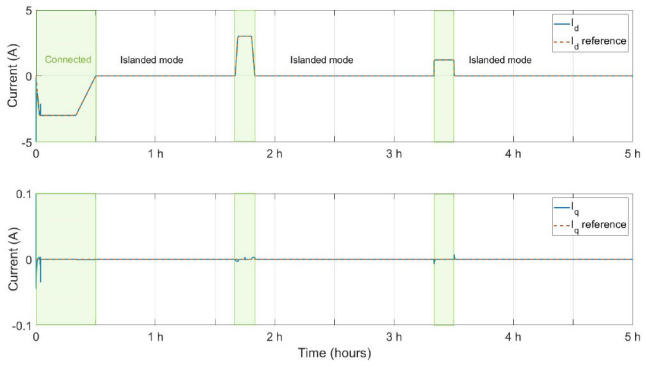

Fig. 10. Currents in AC/DC converter.

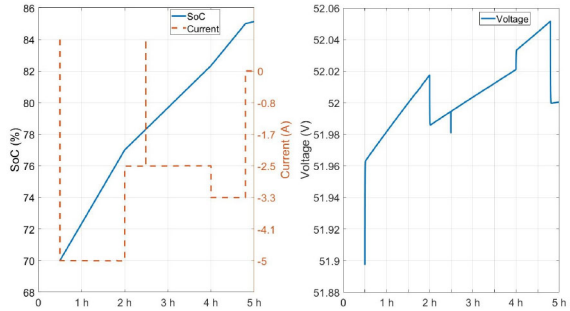

Fig. 11. Battery at node 6.

The AC currents in the three phases AC/DC converter of node 2 in the $dq0$ frame are shown in Figure 10. In Figure 10a, the current i_d does not exist if the DC Microgrid is operating in islanded mode (thus resulting with a value of zero in the figure) and results to track its reference when the DC Microgrid is connected to the AC one. For example, between $0 \leq t \leq 30$ minutes, the reference given by the secondary controller to the AC/DC converter at node 2 is to absorb energy from the AC side ($i_d < 0$) to compensate the lack of renewable energy in the DC Microgrid. On the other hand, in Figure 10b the current i_q is shown. Similarly to the i_d case, it does not take place in islanded mode (thus resulting with a value of zero in the figure). Also, it tracks a zero reference when the DC Microgrid is connected to the main AC grid. Finally, we remark that this type of converter can operate in the fourth quadrants of power operation.

Figure 11 depicts the SoC, current and voltage of the battery at node 6 for the whole simulation. Three different steps are clearly described; fast recharge ($5A$) at the beginning, then slow recharge ($2.5A$), and finally constant voltage in order to not damage the cells in the final step of the recharge process, as usually the battery manufacturers suggest.

In order to better appreciate the proposed nonlinear control laws that acts on milliseconds, Figure 12 shows a zoom at $t = 7200$ seconds (2 hours) of the current in the battery at node 6, as well as the duty cycle of the associated power converter. It is then possible to see how the controller reacts fast to the reference change from fast to slow charge mode taking place at $t = 7200$, then achieving the current to correctly track its reference in only 10 ms. Figure 12b shows that the error between the current an its reference is bounded and always kept very small. In Figure 12c, the duty cycle is shown.

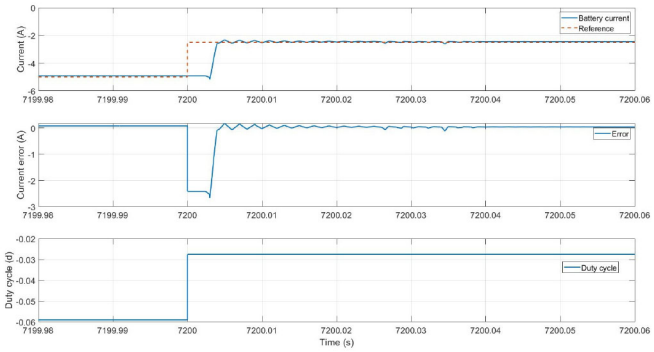

Fig. 12. a) Current in DAB converter in node 6; b) Error; c) Duty cycle.

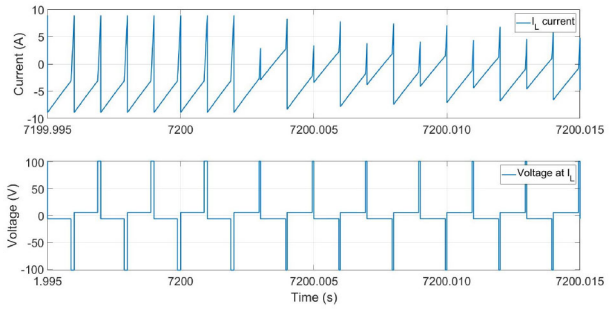

Fig. 13. Current & voltage in the inductance of the DAB in node 6.

Finally, the current in the inductance of the DAB converter in node 6 is shown in Figure 13a. More specifically, a zoom of the simulation time around $t = 7200$ second (2 hours) is depicted, which reflects the change of reference. Both before and after it, with the variables of the converter that are in steady-state, we remark that the average value of this current is zero; consequently, as desired the coil saturation is avoided. On the other hand, Figure 13b shows the voltage in the inductance. It is possible to see that the change of reference alters the curve shape; however, in steady-state the average value of this voltage is also zero.

Consequently, and thanks to what commented above, it is possible to state that the proposed control action fits the target to properly control the several subsystems composing the DC Microgrid, as shown in simulations, both when it operates in islanded mode and when it provides ancillary services to the AC grid. Moreover, the simulations showed that the suggested control approach works in case of plug&play of EVs, and in case of changing the values for the droop gains.

V. Conclusion

This work proposes a droop-inspired nonlinear control strategy for DC Microgrids dedicated to EVs and renewables integration, with no needs for large storage infrastructure, and enables the possibility for the DC Microgrids to provide ancillary services to the Distribution System Operators. A 25 kW DC Microgrid is analysed in MATLAB/Simulink environment, where a PV solar facility of 10 kWp, different types of batteries of EVs in vehicle-to-grid mode of operations as well as a connection to the main AC grid are presented.

The simulations show how the proposed control at local and primary levels stabilizes the voltage of the DC Microgrid while ensuring ancillary services (frequency support) to AC main grid when it is needed. In addition, the DC Microgrid provides a service to end-users as charge station for EVs (light and heavy) with renewable production. Three different control modes are considered for battery chargers (the DAB converters): current control mode (slow or fast), voltage battery constant control mode, and droop control mode to support the DC voltage of the Microgrid. Besides, simulations show the robustness of the proposed controls against intermittent production of energy (renewable) or changes in the number of batteries available in the Microgrid, as well as fast response and high accuracy.

On the other hand, the simulations show that the use of DC Microgrids as EV charging stations can help in the overall stability of the electrical system, where the V2G mode of operation is a key element. Future works will analyse secondary and tertiary controls in order to obtain optimal references as well as the development of a test bench to implement the proposed control laws.

References

[1] E. Veldman and R. A. Verzijlbergh, "Distribution grid impacts of smart electric vehicle charging from different perspectives," *IEEE Trans. Smart Grid*, vol. 6, no. 1, pp. 333–342, Jan. 2015.

[2] L. E. Zubieta, "Are microgrids the future of energy? DC microgrids from concept to demonstration to deployment," *IEEE Electrific. Mag.*, vol. 4, no. 2, pp. 37–44, Jun. 2016.

[3] M. Kumar, S. C. Srivastava, and S. N. Singh, "Control strategies of a DC microgrid for grid connected and islanded operations," *IEEE Trans. Smart Grid*, vol. 6, no. 4, pp. 1588–1601, Jul. 2015.

[4] K.-W. Hu and C.-M. Liaw, "Incorporated operation control of DC microgrid and electric vehicle," *IEEE Trans. Ind. Electron.*, vol. 63, no. 1, pp. 202–215, Jan. 2016.

[5] S. Chandler, J. Gartner, and D. Jones, "Integrating electric vehicles with energy storage and grids: New technology and specific capabilities spur numerous applications," *IEEE Electrific. Mag.*, vol. 6, no. 3, pp. 38–43, Sep. 2018.

[6] P. Grahn, J. Munkhammar, J. Widén, K. Alvehag, and L. Söder, "PHEV home-charging model based on residential activity patterns," *IEEE Trans. Power Syst.*, vol. 28, no. 3, pp. 2507–2515, Aug. 2013.

[7] T. He, Y. Bai, and J. Zhu, "Optimal charging strategy of electric vehicles customers in a smart electrical car park," in *Proc. 8th IET Int. Conf. Power Electron. Mach. Drives (PEMD)*, 2016, pp. 1–6.

[8] W. Wu *et al.*, "A virtual inertia control strategy for DC microgrids analogized with virtual synchronous machines," *IEEE Trans. Ind. Electron.*, vol. 64, no. 7, pp. 6005–6016, Jul. 2017.

[9] S. Sahoo, F. Blaabjerg, and T. Dragicevic, "An adaptive backstepping based virtual inertial control framework for DC microgrids," in *Proc. IEEE 11th Int. Symp. Power Electron. Distrib. Gener. Syst. (PEDG)*, 2020, pp. 85–90.

[10] A. Garcés, *Modeling, Operation, and Analysis of DC Grids*, vol. 1. London, U.K.: Elsevier, 2021.

[11] M. Farrokhabadi *et al.*, "Microgrid stability definitions, analysis, and examples," *IEEE Trans. Power Syst.*, vol. 35, no. 1, pp. 13–29, Jan. 2020.

[12] M. J. Carrizosa, A. Arzandé, F. D. Navas, G. Damm, and J. Vannier, "A control strategy for multiterminal DC grids with renewable production and storage devices," *IEEE Trans. Sustain. Energy*, vol. 9, no. 2, pp. 930–939, Apr. 2018.

[13] L. Mengo *et al.*, "Review on control of DC microgrids and multiple microgrid clusters," *IEEE J. Emerg. Sel. Topics Circuits Syst.*, vol. 5, no. 3, pp. 928–948, Sep. 2017.

[14] Z. Wang and S. Wang, "Grid power peak shaving and valley filling using vehicle-to-grid systems," *IEEE Trans. Power Del.*, vol. 28, no. 3, pp. 1822–1829, Jul. 2013.

[15] M. J. E. Alam, K. M. Muttaqi, and D. Sutanto, "Effective utilization of available pev battery capacity for mitigation of solar PV impact and grid support with integrated V2G functionality," *IEEE Trans. Smart Grid*, vol. 7, no. 3, pp. 1562–1571, May 2016.

[16] W. Zhong, R. Yu, S. Xie, Y. Zhang, and D. K. Y. Yau, "On stability and robustness of demand response in V2G mobile energy networks," *IEEE Trans. Smart Grid*, vol. 9, no. 4, pp. 3203–3212, Jul. 2018.

[17] H. Liang, Y. Liu, F. Li, and Y. Shen, "Dynamic economic/emission dispatch including PEVs for peak shaving and valley filling," *IEEE Trans. Ind. Electron.*, vol. 66, no. 4, pp. 2880–2890, Apr. 2019.
[18] A. Iovine, M. J. Carrizosa, G. Damm, and P. Alou, "Nonlinear control for DC microgrids enabling efficient renewable power integration and ancillary services for AC grids," *IEEE Trans. Power Syst.*, vol. 34, no. 6, pp. 5136–5146, Nov. 2019.
[19] F. Gao, R. Kang, J. Cao, and T. Yang, "Primary and secondary control in DC microgrids: A review," *J. Mod. Power Syst. Clean Energy*, vol. 7, no. 2, pp. 227–242, 2019.
[20] F. Chen, R. Burgos, D. Boroyevich, J. C. Vasquez, and J. M. Guerrero, "Investigation of nonlinear droop control in DC power distribution systems: Load sharing, voltage regulation, efficiency, and stability," *IEEE Trans. Power Electron.*, vol. 34, no. 10, pp. 9404–9421, Oct. 2019.
[21] C. Jin, P. Wang, J. Xiao, Y. Tang, and F. H. Choo, "Implementation of hierarchical control in DC microgrids," *IEEE Trans. Ind. Electron.*, vol. 61, no. 8, pp. 4032–4042, Aug. 2014.
[22] H. Kakigano, Y. Miura, and T. Ise, "Distribution voltage control for DC microgrids using fuzzy control and gain-scheduling technique," *IEEE Trans. Power Electron.*, vol. 28, no. 5, pp. 2246–2258, May 2013.
[23] A. Khorsandi, M. Ashourloo, and H. Mokhtari, "A decentralized control method for a low-voltage DC microgrid," *IEEE Trans. Energy Convers.*, vol. 29, no. 4, pp. 793–801, Dec. 2014.
[24] D. Zonetti, R. Ortega, and J. Schiffer, "A tool for stability and power-sharing analysis of a generalized class of droop controllers for high-voltage direct-current transmission systems," *IEEE Trans. Control Netw. Syst.*, vol. 5, no. 3, pp. 1110–1119, Sep. 2018.
[25] H. K. Khalil and J. Grizzle, *Nonlinear Systems*, vol. 3. Englewood Cliffs, NJ, USA: Prentice Hall, 1996.
[26] A. Iovine, G. Damm, E. De Santis, M. D. D. Benedetto, L. Galai-Dol, and P. Pepe, "Voltage stabilization in a DC microgrid by an ISS-like Lyapunov function implementing droop control," in *Proc. Eur. Control Conf. (ECC)*, 2018, pp. 1130–1135.
[27] E. D. Sontag, *Input to State Stability: Basic Concepts and Results*. Heidelberg, Germany: Springer, 2008, pp. 163–220.
[28] N. Mohan, T. M. Undeland, and W. P. Robbins, *Power Electronics*, Wiley, 1995.
[29] A. R. R. Alonso, J. Sebastian, D. G. Lamar, M. M. Hernando, and A. Vazquez, "An overall study of a dual active bridge for bidirectional DC/DC conversion," in *Proc. IEEE Energy Convers. Congr. Expo.*, 2010, pp. 1129–1135.
[30] M. J. Carrizosa, "Hierarchical control scheme for multi-terminal high voltage direct current power networks," Ph.D. dissertation, Doctorale Sci. Technol., Université Paris-Saclay, Bures-sur-Yvette, France, 2015.
[31] L. Patnaik, A. V. J. S. Praneeth, and S. S. Williamson, "A closed-loop constant-temperature constant-voltage charging technique to reduce charge time of lithium-ion batteries," *IEEE Trans. Ind. Electron.*, vol. 66, no. 2, pp. 1059–1067, Feb. 2019.
[32] Y. Chen, M. J. Carrizosa, G. Damm, F. Lamnabhi-Lagarrigue, M. Li, and Y. Li, "Control-induced time-scale separation for multiterminal high-voltage direct current systems using droop control," *IEEE Trans. Control Syst. Technol.*, vol. 28, no. 3, pp. 967–983, May 2020.
[33] T. Luo, M. J. Dolan, E. M. Davidson, and G. W. Ault, "Assessment of a new constraint satisfaction-based hybrid distributed control technique for power flow management in distribution networks with generation and demand response," *IEEE Trans. Smart Grid*, vol. 6, no. 1, pp. 271–278, Jan. 2015.

Miguel Jiménez Carrizosa received the M.S. Industrial Engineering degree in electrical engineering from the Universidad Politécnica de Madrid (UPM), Madrid, Spain, in 2011, the M.S. degree in energy systems from Supélec, Gif-sur-Yvette, France, in 2011, and the Ph.D. degree in electrical engineering and automatic control from Paris-Sud XI University, Orsay, France, in 2015. He is currently an Assistant Professor with the "Departamento de Energía y Combustibles," Escuela Técnica Superior de Ingenieros de Minas y Energía, UPM, where he is a Researcher with the Centro de Electrónica Industrial. His research interests include HVDC systems, control of power converters, transmission and distribution systems, integration of renewable energies, smart grids, and optimal power flow methods.

Alessio Iovine (Member, IEEE) received the B.Sc. and M.Sc. degrees in electrical engineering and computer science from the University of L'Aquila, L'Aquila, Italy, in 2010 and 2012, respectively, and the European Doctoral degree in information science and engineering from the University of L'Aquila, in collaboration with CentraleSupélec, Paris-Saclay University, Paris, France, in 2016.

From 2016 to 2020, he held postdoctoral positions with the University of L'Aquila, the Efficacity Research Center, France, the University of California at Berkeley, Berkeley, CA, USA, and the CentraleSupélec. He is currently a Researcher with CNRS and a member of L2S, CentraleSupélec, Paris-Saclay University. His research interests include advanced control methods for power and energy systems and traffic control, with smartgrids, integration of renewables and storage devices, autonomous vehicles, and cooperative intelligent transportation systems as core applications. He is a member of the IFAC TC 6.3. on Power and Energy Systems.

Gilney Damm (Member, IEEE) is an Electronic Engineering degree in automatic control from the Rio de Janeiro Federal University, Brazil, and the Ph.D. degree CentraleSupelec—Paris-Saclay University. He is a Senior Research Scientist (Directeur de Recherche) with the Laboratoire COSYS-LISIS, Univ. Gustave Eiffel. His research interests concern nonlinear and adaptive control and observers applied to power systems (SmartGrids, SuperGrid, MicroGrids). His main applications are in the field of large-scale integration of renewable energy and electric vehicles; multiterminal HVDC systems; mixed AC/DC MicroGrids; control of power systems and power electronics in high and low voltage, synchronization of power networks; energy integration in SmartCities. He is a member of the IFAC Technical Committee TC 6.3 Power and Energy Systems since 2015. He has been an Associate Editor of the *European Journal of Control* since 2010.

Pedro Alou (Member, IEEE) was born in Madrid, Spain, in 1970. He received the M.S. and Ph.D. degrees in electrical engineering from the Universidad Politécnica de Madrid (UPM), Spain, in 1995 and 2004, respectively. He is currently a Full Professor and participates in the management of the UPM as a Deputy Vice Chancellor. He has been involved in Power Electronics since 1995, participating in more than 70 R&D projects with the industry. He has authored or coauthored over 50 journal articles, 150 conference papers and holds six patents. His main research interests are in power converters, advanced topologies for efficient energy conversion, modeling of converters and magnetic components, advanced control techniques for high dynamic response, energy management and new semiconductor technologies for power electronics. His research activity is distributed among industrial, aerospace, and military projects.